Published OnlineFirst August 22, 2017; DOI: 10.1158/0008-5472.CAN-17-0925

Molecular and Cellular Pathobiology

Cancer Research

Human Pluripotent Stem Cell–Derived *TSC2*-Haploinsufficient Smooth Muscle Cells Recapitulate Features of Lymphangioleiomyomatosis

Lisa M. Julian[1,2], Sean P. Delaney[1,2,3], Ying Wang[1], Alexander A. Goldberg[4], Carole Doré[1], Julien Yockell-Lelièvre[1], Roger Y. Tam[1,2,5], Krinio Giannikou[6], Fiona McMurray[2,7], Molly S. Shoichet[5], Mary-Ellen Harper[2,3,7], Elizabeth P. Henske[6], David J. Kwiatkowski[6], Thomas N. Darling[8], Joel Moss[9], Arnold S. Kristof[4], and William L. Stanford[1,2,3]

Abstract

Lymphangioleiomyomatosis (LAM) is a progressive destructive neoplasm of the lung associated with inactivating mutations in the *TSC1* or *TSC2* tumor suppressor genes. Cell or animal models that accurately reflect the pathology of LAM have been challenging to develop. Here, we generated a robust human cell model of LAM by reprogramming *TSC2* mutation–bearing fibroblasts from a patient with both tuberous sclerosis complex (TSC) and LAM (TSC-LAM) into induced pluripotent stem cells (iPSC), followed by selection of cells that resemble those found in LAM tumors by unbiased *in vivo* differentiation. We established expandable cell lines under smooth muscle cell (SMC) growth conditions that retained a patient-specific genomic $TSC2^{+/-}$ mutation and recapitulated the molecular and functional characteristics of pulmonary LAM cells. These include multiple indicators of hyperactive mTORC1 signaling, presence of specific neural crest and SMC markers, expression of VEGF-D and female sex hormone receptors, reduced autophagy, and metabolic reprogramming. Intriguingly, the LAM-like features of these cells suggest that haploinsufficiency at the *TSC2* locus contributes to LAM pathology, and demonstrated that iPSC reprogramming and SMC lineage differentiation of somatic patient cells with germline mutations was a viable approach to generate LAM-like cells. The patient-derived SMC lines we have developed thus represent a novel cellular model of LAM that can advance our understanding of disease pathogenesis and develop therapeutic strategies against LAM. *Cancer Res; 77(20); 5491–502. ©2017 AACR.*

Introduction

Lymphangioleiomyomatosis (LAM, OMIM#606690) is a rare, destructive lung disease associated with inactivating mutations in *TSC1* or, more commonly, *TSC2*. LAM arises either sporadically (S-LAM) or due to germline mutations in association with the multisystem neurodevelopmental and tumor disorder tuberous sclerosis complex (TSC-LAM; refs. 1, 2). Found almost exclusively in women, LAM is fundamentally characterized by the progressive growth of microscopic nodules of abnormal smooth muscle–like cells within the lung interstitium, which leads to progressive cystic destruction of the parenchyma, and ultimately respiratory failure (1). The "LAM cells" that grow within these nodules express neural crest lineage markers, predominantly those associated with the smooth muscle cell (SMC) and immature melanocyte lineages, as well as lymphangiogenic proteins and female sex hormone receptors (3–6). LAM patients can also develop renal angiomyolipomas, which similarly express neural crest markers.

TSC2 encodes a GTPase-activating protein that functionally inhibits RHEB, an activator of mTOR complex 1 (mTORC1), which functions as a central regulator of cell growth, proliferation, and survival. Accordingly, TSC2 loss of function (in complex with TSC1 and TBC1D7) and hyperactivation of mTORC1 are defining features of TSC and LAM (1, 2, 4). Aside from lung transplantation, the only clinically approved therapy for LAM is treatment with mTORC1 inhibitors (e.g., rapamycin/sirolimus, everolimus), which slow LAM progression but do not eliminate the disease (7). Improved therapeutic options that eliminate or prevent LAM tumors, particularly those aimed at selectively killing LAM cells, are urgently needed.

A major obstacle limiting the development of effective therapies for LAM is a lack of authentic preclinical models. Although primary TSC2-deficient cells have been isolated from lung biopsies of LAM patients, they cannot be effectively expanded in

[1]Ottawa Hospital Research Institute, Regenerative Medicine Program, Ottawa, Ontario, Canada. [2]University of Ottawa, Ottawa, Ontario, Canada. [3]Ottawa Institute of Systems Biology, Ottawa, Ontario, Canada. [4]Research Institute of McGill University Health Centre, Montreal, Quebec, Canada. [5]University of Toronto, Donnelly Centre for Cellular & Biomolecular Research, Boston, Massachusetts. [6]Division of Pulmonary and Critical Care Medicine, Brigham and Women's Hospital, Harvard Medical School, Boston, Massachusetts. [7]Department of Biochemistry, Microbiology and Immunology, Faculty of Medicine, University of Health Sciences, Bethesda, Maryland. [8]Uniformed Services University of Health Sciences, Bethesda, Maryland. [9]National Heart, Lung, and Blood Institute, NIH, Bethesda, Maryland.

Note: Supplementary data for this article are available at Cancer Research Online (http://cancerres.aacrjournals.org/).

L.M. Julian, S.P. Delaney, and Y. Wang contributed equally to this article.

Corresponding Author: William L. Stanford, Ottawa Hospital, 501 Smyth Road, Box 511, Ottawa, Ontario K1H 8L6, Canada. Phone: 613-737-8899, ext. 75495; Fax: 613-739-6294; E-mail: wstanford@ohri.ca

doi: 10.1158/0008-5472.CAN-17-0925

Published OnlineFirst August 22, 2017; DOI: 10.1158/0008-5472.CAN-17-0925

culture (8). Rodent models of TSC1/2-deficiency (e.g., the Eker rat, *TSC1/2*$^{+/-}$ mice) do not spontaneously develop LAM lung nodules or cysts, and their uterine and renal tumors do not recapitulate the human disease (8, 9). In addition, primary TSC2-deficient cells derived from human patient samples, as well as from many rodent models, typically require viral transformation or p53 deletion for their expansion in culture, and harvested primary tissues are invariably heterogeneous populations of TSC2-deficient and -expressing cells (8). It has thus been difficult to establish homogenous cultures of cells that possess the phenotypes of primary LAM cells. While transformed cell lines have been established from a small number of patient-derived angiomyolipoma tumors (10, 11), they do not optimally reflect the genetic background, lineage identity, and molecular characteristics of LAM cells observed in patients.

Induced pluripotent stem cells (iPSC) have demonstrated tremendous potential for establishing human preclinical models of disease, largely because they can be generated from patient-derived somatic cells, are easily expanded, can be induced to differentiate into multiple lineages, and have shown potential in drug screens (12). We reasoned that iPSC reprogramming of TSC-LAM patient fibroblasts and subsequent differentiation into the SMC lineage would be a promising approach for the generation of a LAM cell model. Thus, in this study, we have established a panel of cell lines that were generated using such a strategy, with dermal fibroblasts from normal-appearing skin and fibroblast-like cells from facial tumors of a TSC-LAM patient (13). These patient-derived cells carry a parental germline *TSC2* mutation and express reduced levels of TSC2. They are expandable in culture, and exhibit widespread molecular and phenotypic characteristics that are consistent with LAM cells. Thus, we provide a novel and highly disease-relevant tool for the study of disease mechanisms and identification of novel therapeutic approaches in LAM.

Materials and Methods

Cell lines and culture

Fibroblasts were maintained in DMEM (Thermo Fisher Scientific, #11965) containing 10% FBS (Gibco, #12483) and 0.5% penicillin–streptomycin (Gibco, 15140-122). SMCs were cultured in 231 medium (Thermo Fisher Scientific, #M231-500) supplemented with 1× smooth muscle growth supplement (Thermo Fisher Scientific, #S-007-25) and 1× gentamycin sulfate (Wisent, #450-135-XL), and in PromoCell phenol red-free smooth muscle cell basal medium 2 (C-22267) for starvation growth conditions. Fibroblasts and SMCs were passaged using 0.05% trypsin-EDTA (Gibco, #25300-054). All iPSC and SMC lines used in this study were generated by the authors from fibroblast cultures and were maintained as described previously (14, 15). Studies with patient cells were performed following approval by the Stem Cell Oversight Committee of Canada and the Institutional Review Board (Ottawa Health Science Network-Research Ethics Board REB #2011706-01H), renewed each year of the study, which operates according to the Declaration of Helsinki and the International Ethical Guidelines for Biomedical Research Involving Human Subjects. Fibroblast lines were obtained with informed consent from: as described in ref. 13 and by the senior author's laboratory in December 2011 (LAM patient-derived), Coriell Institute (000969), ATCC (BJ1C), and Progeria Research Foundation (168; ref. 15) in 2009. H9 ESCs were obtained from WiCell Institute in 2004. All cell lines were authenticated by the authors by genotype and/or Western blot analysis for *TSC2*/tuberin and standard G-banding karyotype analysis (WiCell), and confirmed mycoplasma negative by PCR-based analysis (16). Cryopreserved stocks were established immediately after testing, and experiments were performed within 3–10 passages following thaw of frozen stocks.

iPSC reprogramming

A total of 1×10^5 fibroblasts (cultured without antibiotics for 24 hours) were electroporated with 0.5 μg iPSC episomal vector mixture (17) using a 10 μL kit neon transfection system (Thermo Fisher Scientific; MPK1096; 1,300 V, 20 ms, 2 pulses), and plated into one well of a Matrigel-coated 6-well plate. Cells were cultured in E8 media (18) plus 0.1 μmol/L hydrocortisone until confluency was approximately 20% (typically 5–10 days), at which point cells were cultured in E7 media (E8 without TGFβ) until PSC colonies were visible (typically 25–30 days postelectroporation). Individual colonies were picked and transferred to Matrigel-coated 24-well dishes and expanded and maintained in E8. For *TSC2*-shRNA–transduced fibroblasts, cultures were transferred to E8 + hydrocortisone 48 hours following electroporation.

In vitro differentiation

For embryoid body (EB)-based differentiation, iPSCs were harvested using 1 mg/mL collagenase IV. Small clumps were transferred to ultra-low attachment dishes (Corning Inc.) in E6 media (E8 without TGF-β and bFGF). Medium was changed every day until EBs had formed (typically 7 days), which were then transferred to gelatin-coated plates and cultured for another 7 days before fixation with 4% formaldehyde.

Teratoma assay, tissue preparation, and harvest

iPSCs were dissociated by dispase (Stem Cell Technologies), and 1×10^6 cells resuspended in Matrigel were intramuscularly injected into the tibialis anterior muscles of *NOD/SCID* mice (Charles River Laboratory). These studies were approved by the Animal Care Veterinary Services-University of Ottawa (protocol #OHRIT-1666). Once large visible leg tumors had formed (8–11 weeks), teratomas were dissected and representative tissue was either fixed in 4% formaldehyde and embedded in paraffin, or manually dissociated. Paraffin-embedded tissues were sectioned and stained with hematoxylin and eosin or by IHC. To isolate and expand SMCs in culture, manually dissociated tissue was further dissociated with trypsin-EDTA at 37°C for 20 minutes, washed and centrifuged at 1,000 rpm for 10 minutes, and cultured for multiple passages in SMC growth media on tissue culture–treated plastic or Matrigel (for isolation and early passages only).

shRNA-mediated TSC2 knockdown

Fibroblasts and SMCs were transduced with dual-cistronic lentiviral vectors engineered to express both turboGFP and human *TSC2*-targeted [or scrambled control (Control)] shRNA sequences in the presence of doxycycline (GE Dharmacon SmartChoice lentiviral line; *TSC2*-sh1, VSH6376-220794900; *TSC2*-sh2, VSH6376-220794908; scrambled control, VSC6572). shRNA expression was induced by adding freshly dissolved 500 μg/mL (fibroblasts) or 1 mg/mL (SMCs) doxycycline to the culture media for a minimum of 7 days prior to iPSC reprogramming or harvest/analysis. shRNA expression was maintained throughout the entire course of reprogramming.

Published OnlineFirst August 22, 2017; DOI: 10.1158/0008-5472.CAN-17-0925

Extracellular flux assays

Oxygen consumption and extracellular acidification rates (OCR and ECAR, respectively) were measured using a Seahorse XF-24 bioanalyzer (Agilent Technologies). A total of 6.5×10^4 live cells were plated per well in a Matrigel-coated 24-well dish (Agilent Technologies, 100882-004) 18–24 hours prior to experiments. Concentrations of molecules used in the mitochondrial stress test and glycolysis assays were as follows: FCCP (1 μmol/L), oligomycin (1 μg/mL), antimycin A (1 μmol/L), rotenone (0.5 μmol/L), glucose (10 mmol/L), 2-deoxyglucose (100 mmol/L). OCR and ECAR were normalized to total cell protein; OCR was also corrected for nonmitochondrial respiration.

mTORC1 and autophagy inhibitor treatments

For rapamycin and chloroquine experiments, SMCs were cultured in SMC growth media until approximately 60% confluent and were treated with 10 nmol/L rapamycin (Calbiochem, #553211), 5 μmol/L chloroquine (Sigma, #C6628), or vehicle (DMSO at 1/1,000) in basal DMEM (Gibco, #11054-020) for 24 hours. Cells were then harvested for flow cytometry analysis (for each sample, media- and trypsin-harvested adherent cells were combined). Cells were stained with propidium iodide (PI; 50 ng per 5×10^4–1×10^5 cells) and analyzed for PI staining via flow cytometry. For bafilomycin A1, torin-1, rapamycin experiments: cells were treated with 2 nmol/L torin-1 (Millipore, #475991), 50 nmol/L rapamycin (or DMSO for controls) for 4 hours, and then with 250 nmol/L bafilomycin A1 (or DMSO for controls; Enzo Life Sciences, # BML-CM110-0100) for an additional 2 hours. Cells were then harvested into protein lysis buffer for Western blot analysis.

Statistical analysis

Statistical analyses to assess differences across groups were performed using one-way ANOVA or two-tailed Student *t* test, where indicated. Where ANOVA analysis revealed significant differences, a Tukey *post hoc* test was used for pairwise comparisons. Error bars represent SEM. *P* values of <0.05 (*), <0.01 (**), and <0.001 (***) were considered statistically significant.

Additional information can be found in Supplementary Materials and Methods.

Results

Generation and characterization of TSC-LAM patient-derived iPSCs

Low-passage dermal fibroblasts were grown from explants from either facial tumor tissue or normal-appearing skin (tissue adjacent to visible tumors) obtained from two women with TSC and clinical manifestations of LAM. Next-generation sequencing revealed that Patient 6 (P6) carries a *TSC2* germline mutation with two additional second-hit *TSC2* mutations in her angiofibroma-derived fibroblasts, each with allele frequency of less than 0.5 (Supplementary Fig. S1A; ref. 13). Thus, cultures of normal-appearing fibroblasts (Norm-fib) from P6 can be expected to be a homogenous $TSC2^{+/-}$ population. Tumor-derived fibroblasts (Tum-fib) from P6 are likely composed of both $TSC2^{-/-}$ and, as confirmed later, $TSC2^{+/-}$ cells (Fig. 1A). Mutation analysis of blood and fibroblasts grown from Patient 5 (P5) demonstrated that the patient was mosaic for a first-hit *TSC2* mutation, with allele frequency of 0.07 in blood (13). Three tumor-derived fibroblast lines from P5 had second-hit point mutations or deletions at varying allele frequencies (Supplementary Fig. S1A; ref. 13). Cultures from P5 are therefore expected to be heterogeneous mixtures of either $TSC2^{+/+}$, $TSC2^{+/-}$ (Norm-fib) or $TSC2^{+/+}$, $TSC2^{+/-}$, $TSC2^{-/-}$ (Tum-fib lines) cells (Fig. 1A). Consistent with TSC2 deficiency and concomitant mTORC1 hyperactivation in tumor-derived cells, TSC2 protein expression was substantially reduced and levels of phosphorylated S6 (P-S6) were elevated in all tumor cell lines compared with the normal-appearing fibroblasts for each patient (Supplementary Fig. S1B; ref. 13).

To determine whether TSC-LAM somatic cells are able to acquire a pluripotent state, patient-derived fibroblast lines were subjected to epigenetic reprogramming. Morphologic changes suggestive of mesenchymal-to-epithelial transition were noticeable by day 5 posttransduction, and colonies resembling those formed by human embryonic stem cells (hESC) were visible by days 20–25. hESC-like colonies were obtained from all sources except for the P5 angiofibroma Nose-Tum-fib cells (Fig. 1A). A subset of colonies was manually harvested and subcultured in individual Matrigel-coated wells at day 30 posttransduction, and these have now maintained an undifferentiated hESC-like morphology for over 25 passages (Fig. 1B). We randomly selected 2–3 clones from each group and performed standard iPSC characterization assays. Most lines possessed a karyotype identical to that of the parental fibroblasts (Supplementary Fig. S2A and S2B; lines with abnormal karyotypes were excluded from further study), all lines expressed classical pluripotency markers (Fig. 1C; Supplementary Fig. S3A and S3B), and most were capable of differentiating into cells that express markers of all three germ layers *in vitro* and *in vivo* (Supplementary Fig. S3A–S3E). The one exception is that P6 tumor–derived iPSCs were unable to generate $GATA6^+$ endoderm lineage cells.

TSC2 deficiency inhibits iPSC reprogramming

In all but one case (P5 FH-Tum-fib) the tumor-derived fibroblasts gave rise to fewer colonies than did the normal-appearing dermal cells from each patient (Fig. 1A), suggesting that complete loss of TSC2 represents a barrier to somatic cell reprogramming to pluripotency. Genotyping analysis revealed that while all iPSC colonies derived from P6 carried the first-hit *TSC2* germline mutation found in the parental cell lines (*TSC2* c.4375C>T, p. R1459*), none of the second-hit mutations observed in the tumor-derived fibroblasts were present (Supplementary Fig. S4A and S4B). Thus, the P6 iPSC lines are genotypically $TSC2^{+/-}$; accordingly, they each express *TSC2* at half-maximal levels compared with wild-type (WT) controls (Fig. 1D). No *TSC2* mutations were identified in colonies derived from the mosaic dermal cultures of P5 (Supplementary Fig. S4B and S4C).

We attempted to reprogram two additional cell sources that are widely considered to be TSC2-deficient: the human renal angiomyolipoma-derived 621-101 cell line (11) and primary LAM patient lung explants isolated at the time of double lung transplant. The latter typically yield *TSC2* genetically heterogenous cultures. The 621-101 cells gave rise to partially reprogrammed colonies that were unstable and could not be reestablished from cryopreserved samples. All iPSC lines generated from the lung explants demonstrated normal TSC2 (and TSC1) expression. To directly test the hypothesis that TSC2 deficiency inhibits reprogramming, we used a doxycycline-inducible shRNA approach to knock down *TSC2* in otherwise normal fibroblasts and performed subsequent iPSC reprogramming experiments. As expected, reduction of *TSC2* expression to 36%–45% of normal

Published OnlineFirst August 22, 2017; DOI: 10.1158/0008-5472.CAN-17-0925

A

Patient ID	Fibroblasts ID	Fibroblasts genotypes	*#iPSC colonies/ 10^4 fibroblasts*	iPSC sub-clones ID	iPSC Genotypes
Patient 6	Norm-fib	*TSC2+/-*	7	P6N1, P6N2	*TSC2+/-*
	Tum-fib	*TSC2+/-; TSC2-/-*	0.15	P6T1, P6T2	*TSC2+/-*
Patient 5	Norm-fib	*TSC2+/+; TSC2+/-*	1.2	P5N1, P5N2, P5N3	*TSC2+/+*
	Mouth-Tum-fib	*TSC2+/+; TSC2+/-; TSC2-/-*	0.5	P5MT1, P5MT2, P5MT3	*TSC2+/+*
	Forehead (FH)-Tum-fib	*TSC2+/+; TSC2+/-; TSC2-/-*	3.2	P5FHT1, P5FHT2, P5FHT3	*TSC2+/+*
	Nose -Tum-fib	*TSC2+/+; TSC2+/-; TSC2-/-*	0	*NA*	*NA*

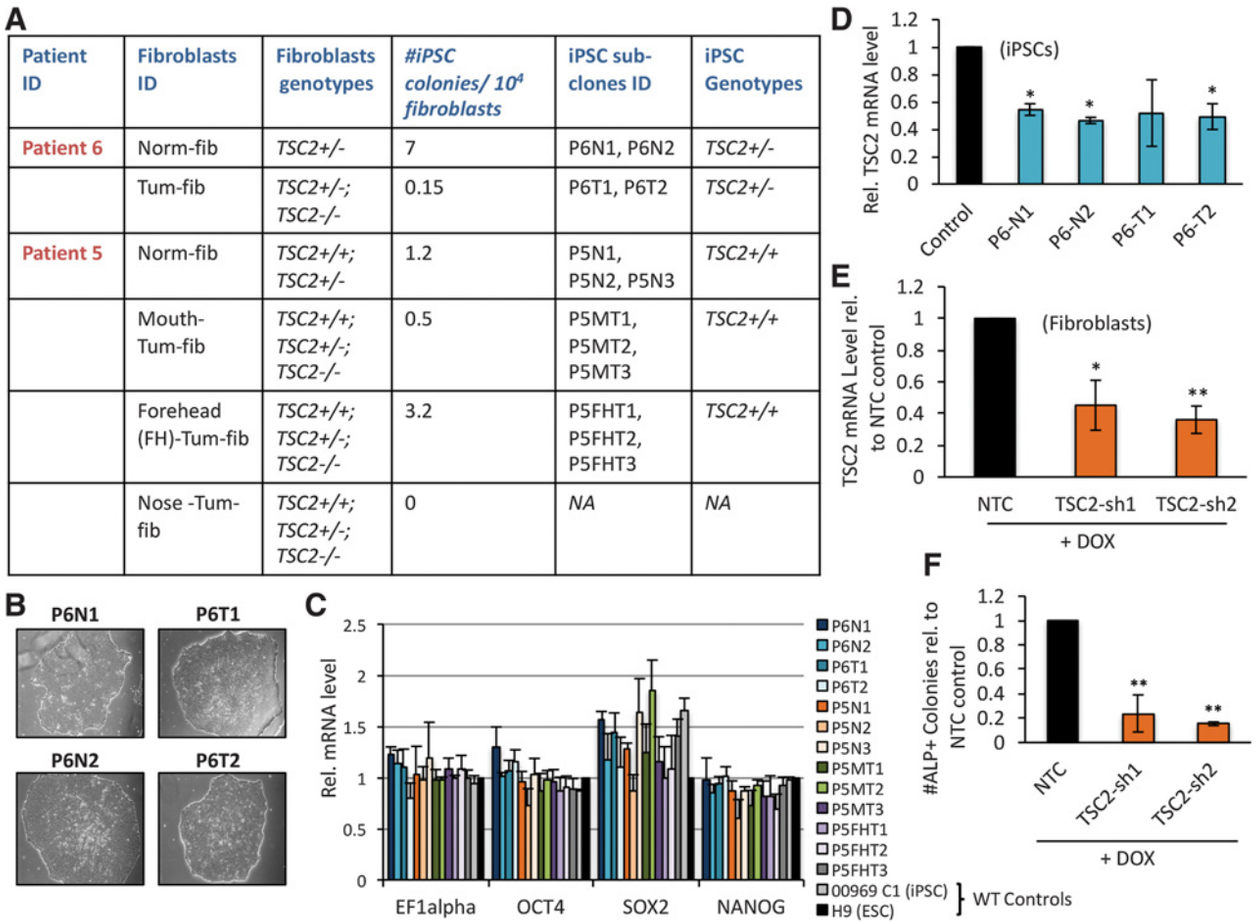

Figure 1.

TSC2 deficiency inhibits iPSC reprogramming. **A,** *TSC2* genotypes of patient-derived fibroblasts and derivative iPSC subclones used in this study, as well as frequency of iPSC reprogramming of patient-derived fibroblasts. **B,** Representative phase-contrast images of Patient 6 (P6)-derived iPSC colonies. **C,** qRT-PCR analysis of mRNA levels of pluripotency markers (indicated along *x*-axis) in control and patient-derived iPSC lines, expressed as relative (Rel.) to wild-type (WT) H9 ESCs for each indicated gene. **D,** qRT-PCR for *TSC2* in P6-derived iPSCs relative to nonpatient control cell line "168." Relative *TSC2* expression (**E**) and number of alkaline phosphatase (ALP)–positive iPSC colonies (**F**) in 090 fibroblasts carrying *TSC2* shRNAs ("TSC2-sh1" and "TSC2-sh2") or a scrambled "control" RNA molecule, following Dox-induced shRNA expression. Data in **E** and **F** are expressed as relative to scrambled "control" cells. Statistics are relative to the following controls: H9 ESCs (**C**), 168 iPSCs (**D**), and scrambled controls (**E** and **F**). *, $P < 0.05$; **, $P < 0.01$ are indicated. Three biological replicates were performed for each experiment.

levels (Fig. 1E) resulted in a substantially reduced number of reprogrammed iPSC colonies (Fig. 1F).

Establishment of TSC-LAM patient-derived smooth muscle cells

Considering the possibility that iPSC lines derived from tumor biopsies may have retained an epigenetic memory of their original tumor microenvironment (19), we tested whether the normal dermal- and tumor-derived iPSCs adopt distinct cellular phenotypes upon *in vivo* differentiation. We injected representative tumor and normal tissue-derived iPSCs from P5 ($TSC2^{+/+}$) and P6 ($TSC2^{+/-}$), as well as control iPSCs derived from individuals without TSC or LAM, into immunodeficient mice for teratoma growth and subsequent analysis of differentiated tissues. All iPSC lines gave rise to teratomas over a similar time frame, and grew to a similar size with comparative multipotent differentiation potential (Supplementary Fig. S3D and S3E).

Given a potential pathogenic role for $TSC2^{+/-}$ cells in TSC and LAM lesions (20–23), we focused on two tumor-derived (P6T1, P6T2) and two normal-appearing dermal-derived (P6N1, P6N2) P6 $TSC2^{+/-}$ iPSC lines. Overall, these cell lines demonstrate elevated mTORC1 signaling, evidenced by increased phosphorylation of S6 kinase (P-S6K) compared with WT nonpatient iPSC controls (969B and 168; Fig. 2A). We reasoned that it may be possible to isolate disease-relevant LAM cells by culturing tumor explants under growth conditions selective for the putative cell type of interest. Given the pervasive expression of SMC markers in LAM lung and kidney lesions, we predicted that isolation of teratoma-derived SMCs would select for LAM-like cells. To investigate this, we cultured a portion of each P6-derived teratoma directly under SMC growth conditions (Fig. 2B). Robust cell cultures morphologically similar to SMCs were quickly established from the P6 teratoma-derived tissue (Fig. 2C; designated fibroblast tumor-derived lines P6T1-SMC and P6T2-SMC, and

Published OnlineFirst August 22, 2017; DOI: 10.1158/0008-5472.CAN-17-0925

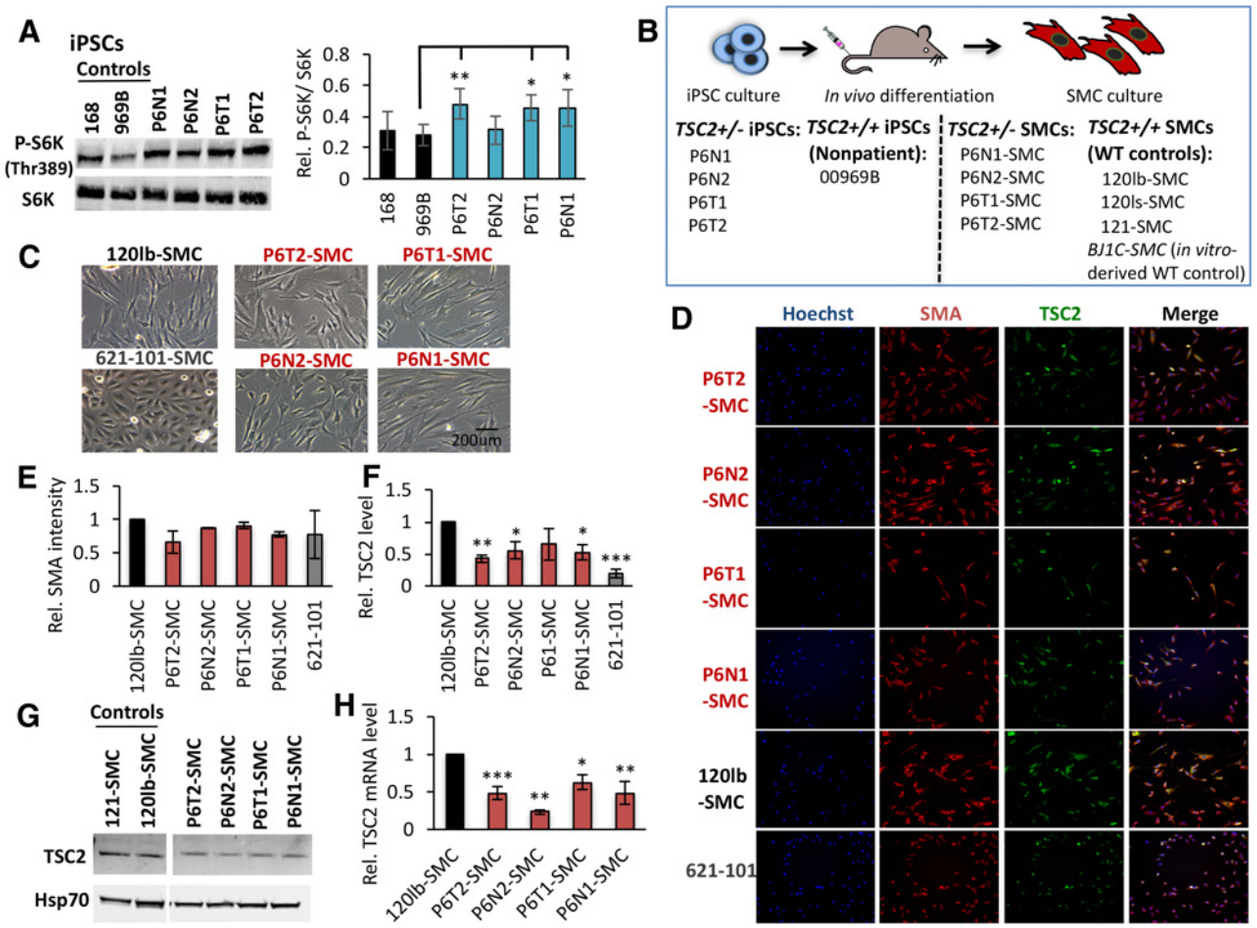

Figure 2.

Establishment of TSC/LAM patient-derived SMC lines. **A,** Representative Western blot analysis and densitometry quantification, expressed as relative to control cell line 969B, of total and phosphorylated (P-S6K, Thr389) S6K in control and P6 iPSC lines. **B,** Four P6 iPSC lines (as indicated), and one nonpatient WT control iPSC line (969B, as indicated), were injected intramuscularly for *in vivo* differentiation in teratomas, and explants were cultured under SMC growth conditions. The four SMC patient-derived lines and three SMC WT control lines that were established using this approach are indicated. Note we also use a fourth WT control SMC line in this study, BJIC-SMC, which was generated by *in vitro* differentiation of nonpatient iPSCs. Representative phase contrast (**C**) and high content imaging immunofluorescence [smooth muscle actin (SMA), TSC2; **D**] images of P6-derived, 120lb-SMC control and 621-101 cells. Quantification of high content imaging images for mean intensity of SMA (**E**) and TSC2 (**F**) proteins, expressed as relative to 120lb-SMC controls, as well as Western blot for TSC2 (**G**), in cultured cell lines. **H,** *TSC2* mRNA expression relative to 120lb-SMCs. Statistics are relative to 969B (**A**) and 120lb-SMC (**E**, **F**, **H**) controls. *, $P < 0.05$; **, $P < 0.01$; and ***, $P < 0.001$ are indicated where statistical differences were observed. A minimum of three biological replicates was performed for each experiment.

normal dermal tissue-derived lines P6N1-SMC and P6N2-SMC; Fig. 2B). WT control SMC lines were established by culturing a representative portion of teratoma tissue derived from non-TSC/LAM 00969B iPSCs (120lb-SMC, 120ls-SMC, 121-SMC; Fig. 2B), or via directed *in vitro* differentiation of iPSCs into the SMC lineage (BJ1C-SMC; Fig. 2B; ref. 24). P6-derived cultures maintain SMC-like morphology and growth potential similar to control SMC cultures in excess of 20 passages (greater than 50 population doublings), importantly without requiring viral transformation. Each P6-SMC line expresses the classical smooth muscle cell marker smooth muscle actin at levels comparable with WT controls and the 621-101 cell line (cultured under the same growth conditions; Fig. 2D and E), as determined by quantitative high content imaging. Importantly, TSC2 protein expression is reduced in P6-SMCs, in each case falling at a level in between WT control and $TSC2^{-/-}$ 621-101 cells (Fig. 2D, F, and G). *TSC2* mRNA expression is reduced in P6-SMCs to 23%–63% that of control cells (Fig. 2H).

The reduced levels of TSC2 mRNA and protein in the P6-SMC lines suggest that they have maintained the heterozygous *TSC2* status observed in the iPSC state. Sanger, Snapshot, and next-generation sequencing confirmed the 4375C>T mutation (Supplementary Fig. S1A) at 50% allele frequency in all P6-SMC lines. We tested the possibility that second-hit mutations were acquired during teratoma development; however, our multiple sequencing methods failed to detect any additional *TSC2* mutations or any mutations among a bait set of 49 genes related to the TSC/mTOR pathway. Thus, the P6-SMC lines are genetically similar to the iPSC lines from which they were derived, each carrying the same patient-derived *TSC2* germline mutation.

Published OnlineFirst August 22, 2017; DOI: 10.1158/0008-5472.CAN-17-0925

Patient-derived SMCs exhibit markers of mTORC1 activation

Next, we examined the SMC lines for indicators of hyperactive mTORC1 signaling (Fig. 3A). In P6-SMCs we observed elevated P-S6K to varying degrees and a consequent increase in cell size, classical markers of mTORC1 activation (Fig. 3B and C; refs. 1, 25). Cells in which *TSC2* expression was further reduced by doxycycline-inducible shRNA targeting exhibited a greater increase in size (Supplementary Fig. S5A–S5C), suggesting that the $TSC2^{+/-}$ SMCs display an intermediate response to mTORC1 activation. Also reflecting elevated mTORC1 signaling and TSC2 deficiency (26), we observed impaired autophagic flux in P6-SMCs, indicated by reduced accumulation of the lipidated form of LC3B (LC3B-II) in the presence of the lysosomal acidification inhibitor bafilomycin A1 (Fig. 3D). HIF1α protein levels were elevated in a subset of P6-SMC lines compared with control cells (Fig. 3E) and, as expected, were attenuated by treatment with the mTORC1 inhibitor rapamycin (Fig. 3F). Thus, $TSC2^{+/-}$ P6-SMCs demonstrate canonical features of hyperactive mTORC1 signaling.

Patient-derived SMCs exhibit known biomarkers of LAM

Pulmonary LAM cells express neural crest lineage markers, including the melanoma-associated antigens ganglioside D3 (GD3) and glycoprotein 100 (gp100), identified by HMB45 antibody (4, 27–31). We find that under serum starvation conditions, where mTORC1 activity should normally be repressed, tumor-derived and P6N2-SMC lines express GD3 at a high frequency (48%–56% $GD3^+$), whereas WT control SMC or 621-101 cultures have substantially fewer $GD3^+$ cells (8%–15% $GD3^+$; Fig. 4A and B). Immunofluorescence for gp100 revealed a typical cytoplasmic, largely punctate staining pattern in a minority of cells in P6-SMCs (Supplementary Fig. S6A); gp100 was also detected via IHC in a subset of cells (Supplementary Fig. S6B). Low staining in 621-101s was also observed,

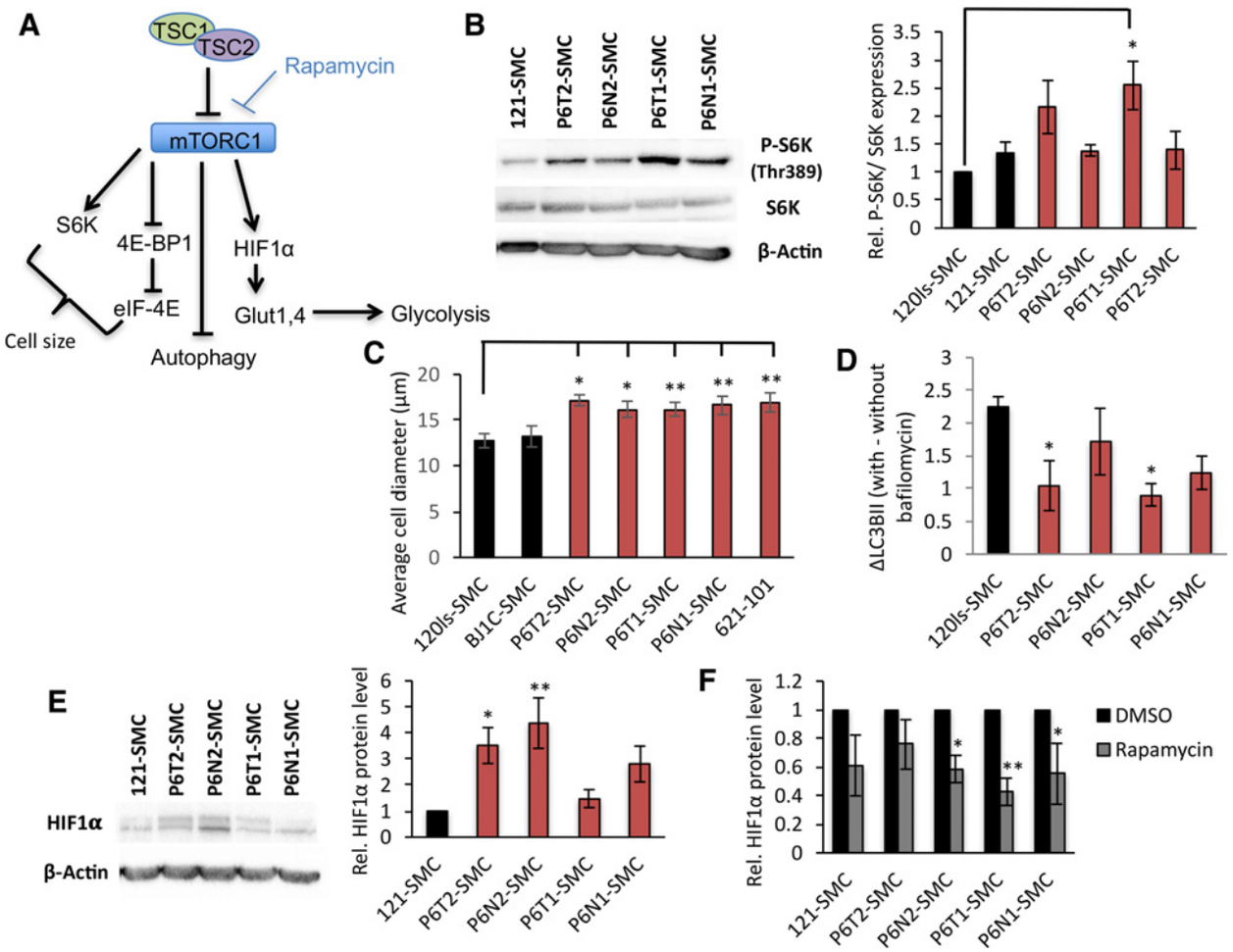

Figure 3.

Patient-derived SMC lines exhibit hyperactive mTORC1 signaling. **A,** Simplified mTORC1 signaling network. **B,** Representative Western blot analysis for pan-S6K and its T389 phosphorylated form (P-S6K) in SMC lines, and densitometry-based quantification expressed as relative to control 120ls-SMCs. Average diameter of cells (**C**) and change in LC3B-II levels with or without bafilomycin A1 (**D**) in SMC lines. **E,** Western blot analysis for HIF1α (left) and densitometry-based quantification (right) expressed as relative to 121-SMC control. **F,** Densitometry-based quantification of Western blots for HIF1α expression in SMC lines in the presence of DMSO (vehicle) or rapamycin, expressed as relative to the DMSO condition for each cell line. Statistics are relative to 120ls-SMC (**B–D**), 121-SMC (**E**), and DMSO condition (**F**; *t* test). *, $P < 0.05$ and **, $P < 0.01$ are indicated. A minimum of three biological replicates was performed for each experiment.

Published OnlineFirst August 22, 2017; DOI: 10.1158/0008-5472.CAN-17-0925

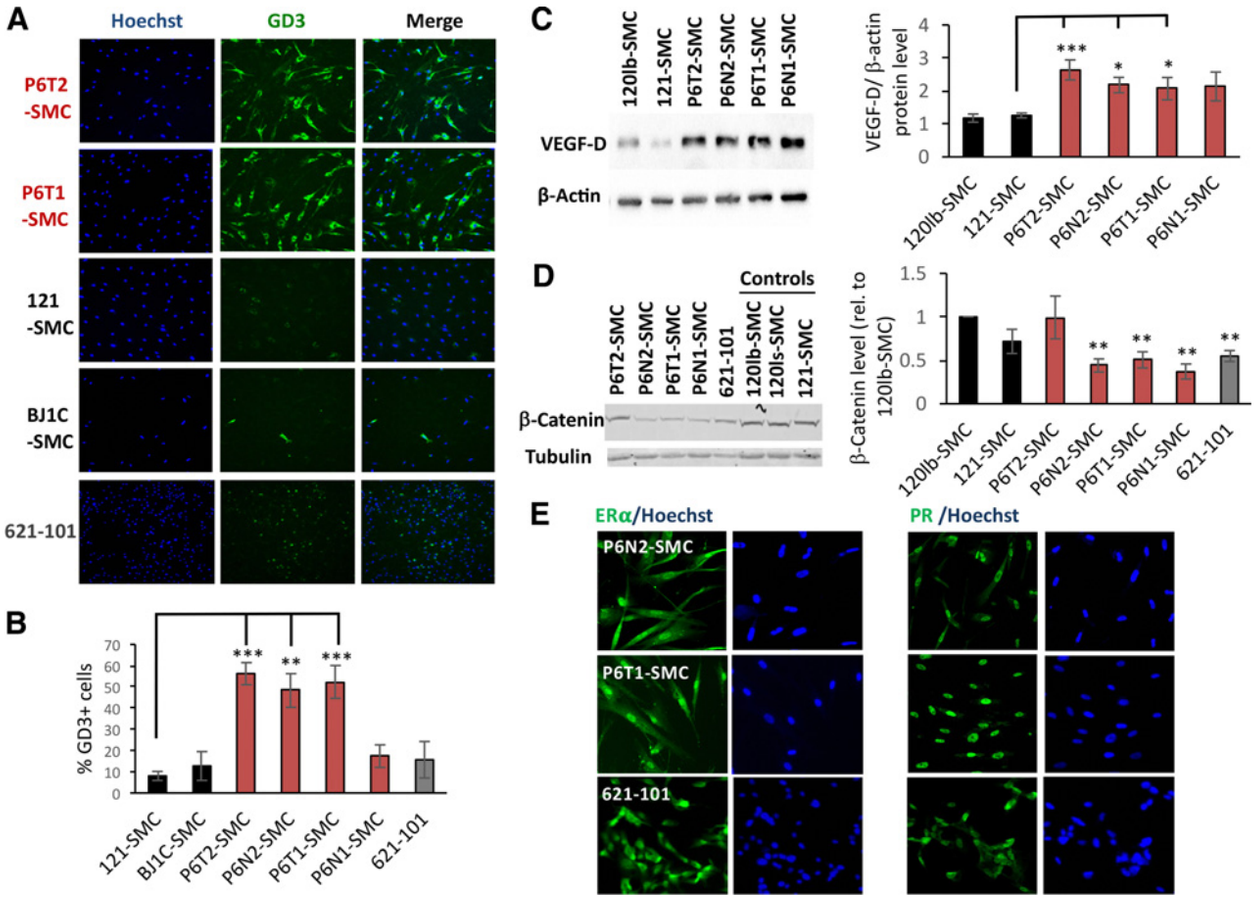

Figure 4.

Patient-derived SMCs exhibit known LAM cell biomarkers. **A,** High content imaging for ganglioside D3 (GD3) and Hoechst nuclear stain in control (121-SMC, BJ1C-SMC), P6-SMC, and 621-101 cell lines, with representative quantification (**B**). **C,** Representative Western blots and densitometry quantification (expressed as VEGF-D levels normalized to β-actin expression) for VEGF-D in P6-SMC and control (120lb-SMC, 121-SMC) lines. **D,** Representative Western blots and densitometry quantification (normalized to tubulin and expressed as relative to 120lb-SMC control) for β-catenin in P6-SMC and control (120lb-SMC, 120ls-SMC, 121-SMC) lines. **E,** Representative immunofluorescence images for estrogen receptor alpha (ERα) and progesterone receptor (PR), and the corresponding Hoechst images, in P6-SMC lines and 621-101 cells. Statistics are relative to 121-SMC (**B** and **C**) and 120lb-SMC (**D**) controls. *, $P < 0.05$; **, $P < 0.01$; and ***, $P < 0.001$ are indicated. A minimum of four and up to seven biological replicates was performed for each experiment.

and while visibly higher in P6-SMCs compared with WT and nonspecific antibody control conditions, gp100 staining intensity did not substantially increase in response to further reduction of *TSC2* expression in P6-SMCs (Supplementary Fig. S6A). This low and heterogenous level of staining in the proliferative P6-SMC cultures may reflect the inverse correlation between gp100 and PCNA levels (i.e., proliferation) previously observed in LAM nodules (29, 31–33).

Intriguingly, in P6-SMCs levels of the lymphangiogenic factor VEGF-D, an important diagnostic biomarker for LAM (34, 35), were 2-fold higher than in controls (Fig. 4C). Reduced levels of β-catenin were also observed in both the 621-101 and P6-SMC lines (Fig. 4D), a phenotype recently reported in TSC2-deficient melanocytes (36). Consistent with the female preponderance of LAM, P6-SMCs exhibited pervasive expression of progesterone receptor (PR) and estrogen receptor alpha (ERα; Fig. 4E; refs. 3–6), which notably did not appear to change with further *TSC2* reduction (Supplementary Fig. S6C). Thus, P6-SMCs exhibit the majority of molecular phenotypes found in LAM cells *in situ*, notably to a greater degree than the 621-101 angiomyolipoma-derived cell line (Table 1).

Glycolytic metabolic reprogramming in *TSC2*$^{+/-}$ SMCs

Like cancer cells, TSC2-deficient cells are characterized by an atypical dependence on glycolytic metabolism at the expense of mitochondrial oxidative phosphorylation (4, 37, 38). Reflecting this, P6-SMC lines exhibited increased expression of the glycolytic enzymes *GLUT1*, enolase, and *G6PDH* compared with both WT controls and 621-101 cells (Fig. 5A–C). Importantly, G6PDH is associated with flux through the pentose phosphate pathway, a phenotype previously associated with TSC2-deficient cells (39). Correspondingly, levels of the *PGC1α* transcription factor, which is indicative of flux through the mitochondrial electron transport chain (ETC), were substantially reduced in the P6 tumor–derived and P6N2 SMC lines (Fig. 5D).

To directly test for a glycolytic phenotype in P6-SMCs, we performed a series of cellular energetics assays designed to test responses to stimulation or perturbation of mitochondrial and

Published OnlineFirst August 22, 2017; DOI: 10.1158/0008-5472.CAN-17-0925

Table 1. Summary of LAM cell phenotypes observed in *TSC2*$^{+/-}$ patient-derived SMC lines and 621-101 cells

	Cell line ID:	621-101	P6N1-SMC	P6N2-SMC	P6T1-SMC	P6T2-SMC
TSC2 loss	Reduced TSC2 expression	✔	✔	✔	✔	✔
	SMC marker expression	✔	✔	✔	✔	✔
LAM/ TSC markers	Elevated GD3 levels	✗	✗	✔	✔	✔
	Elevated VEGF-D levels	✗	✗	✔	✔	✔
	Aberrant β-Catenin expression	✔	✔	✔	✔	✗
	ER-α, PR expression	✔	✔	✔	✔	✔
	gp100 expression	---	---	ND	---	---
mTOR activation	Increased P-S6/ P-S6K, cell size	✔	✔	✔	✔	✔
	Rapamycin responsiveness	✔	✔	✔	✔	✔
	Glycolytic metabolism	ND	✔	✔	✔	✔
	Reduced autophagy	ND	✔	✗	✔	✔
	Sensitivity to mTOR + autophagy inhibition	✗	✗	✗	✔	✔

NOTE: Checkmarks, *x*-marks, and "ND" indicate, respectively, that the phenotype was observed, not observed, and not determined. "---" indicates that positive staining for gp100 was detected, but in a small subpopulation of cells.

glycolytic metabolic pathways. Compared with P6-SMCs, control cell lines exhibited a higher resting OCR as well as an increased maximal respiratory capacity (OCR in the presence of the ATP synthase inhibitor oligomycin and ETC chemical uncoupler FCCP; Fig. 5E). This is due to a higher ATP production in control lines (based on reduction in OCR levels following the addition of oligomycin; Fig. 5F). We observed a significantly higher ECAR in the P6N2 and tumor-derived SMC lines compared with controls under both glucose-free and glucose-stimulated conditions; ECAR was also elevated in P6-SMC lines following ATP synthase inhibition (Fig. 5G). Thus, P6-SMCs exhibit an increased glycolytic metabolic phenotype, in contrast to the aerobic state of WT control cells.

Combined autophagy and mTORC1 inhibition selectively sensitizes tumor-derived SMCs to cell death

Cellular macroautophagy is tightly regulated by mTORC1 activity, leading to speculation that the cytostatic but noncytotoxic effects of rapamycin on LAM cells are due to enhanced autophagy via metabolic reprogramming (1, 4, 40). Indeed, a degree of dependency on autophagy for cell survival in the context of rapamycin treatment has been demonstrated *in vivo* using both xenograft and transgenic mouse TSC models (26). We found reduced autophagic flux in P6-SMCs (Fig. 3D), and show here that basal LC3B-II levels become elevated in these cells when mTOR is inhibited by rapamycin or torin-1 (Fig. 6A and B). This suggests that autophagy is regulated in an mTORC1-dependent manner in P6-SMCs, and specifically that autophagy is elevated in these cell lines in the presence of mTORC1 inhibitors.

We next sought to address whether these autophagy signaling dynamics could be exploited in a therapeutic context to selectively kill these cells in combination with rapamycin treatment, as has been previously shown in the murine TSC2-deficient ELT3 cell line (26). To test this strategy, we treated WT control, 621-101, and P6-SMC lines with rapamycin and the autophagy inhibitor chloroquine, either alone or in combination, and assessed cell death 24 hours later. First, P6-SMCs exhibited increased viability under basal growth conditions compared with controls (Supplementary Fig. S7). Culturing these cells for 24 hours in serum- and nutrient-deficient ("starved") media did not affect cell viability on its own (Supplementary Fig. S7). Moreover, treatment with either rapamycin or chloroquine alone under starved conditions did not

Published OnlineFirst August 22, 2017; DOI: 10.1158/0008-5472.CAN-17-0925

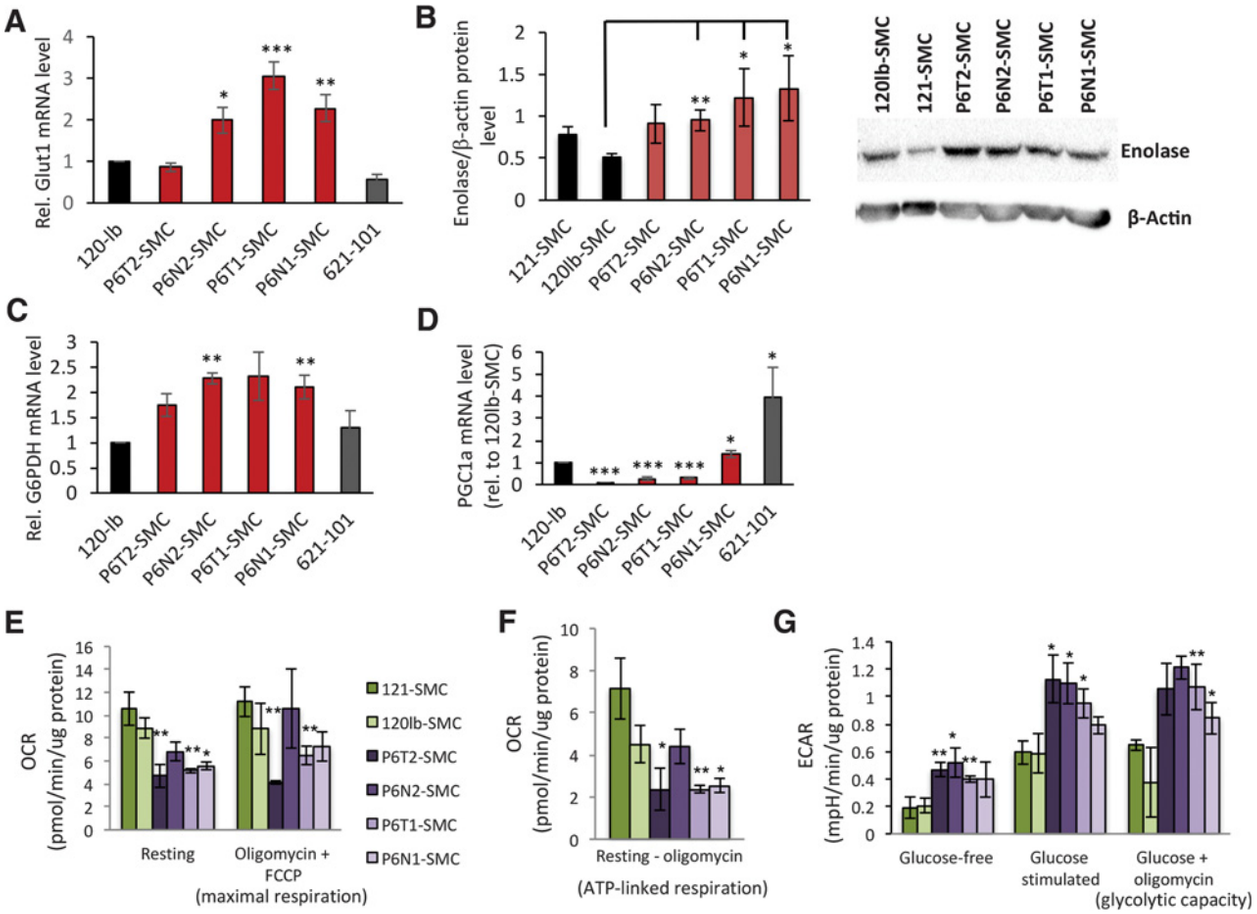

Figure 5.

TSC2$^{+/-}$ SMCs exhibit metabolic reprogramming to a glycolytic state. **A,** qRT-PCR analysis of *GLUT1* expression in SMC lines and 621-101 cells, expressed as relative to 120Ib-SMC control. **B,** Representative Western blot (bottom) and densitometry-based quantification (top) of enolase expression (plotted are enolase levels normalized to β-actin levels) in SMC lines. qRT-PCR analysis of *G6PDH* (**C**) and *PGC1a* (**D**) expression in SMC lines (expressed as relative to 120Ib control cells). Statistics for **A–D** are relative to the 120Ib-SMC control line. OCR measurements under resting and maximal respiratory conditions (**E**), and the difference between OCR levels at resting state and following exposure to oligomycin to indicate ATP turnover (**F**). ECAR under glucose-free and maximal (+glucose, +oligomycin) conditions (**G**). For **E–G**, control (green bars) and P6-derived (purple bars) SMC lines were normalized to total protein as indicated. Statistics are relative to the average of the two control lines. *, $P < 0.05$; **, $P < 0.01$; and ***, $P < 0.001$ are indicated. *t* tests were performed for **B** and **G**. A minimum of three biological replicates was performed for each experiment.

significantly reduce viability in any of the lines tested (Fig. 6C). Combination treatment with rapamycin and chloroquine, however, resulted in a significant increase in cell death in the P6 tumor–derived SMC lines, but not those lines derived from the P6 normal tissue, WT control lines, or 621-101 cells (Fig. 6C). Thus, patient tumor-derived SMC lines have specifically retained an autophagy-dependent survival mechanism that is activated upon mTORC1 inhibition.

Discussion

Through epigenetic reprogramming, *in vivo* differentiation, and subsequent SMC lineage selection of dermal cells derived from a TSC-LAM patient, we have generated expandable, nontransformed, human cell lines carrying a *TSC2* mutation that exhibit multiple characteristics of classical LAM cells (summarized in Table 1). In addition to modeling LAM, our work has revealed key features of the role of TSC2 in establishing pluripotency. P6 dermal cultures, which contained both *TSC2*$^{+/-}$ and *TSC2*$^{-/-}$ cells, only gave rise to *TSC2*$^{+/-}$ iPSCs, and the mosaic P5 dermal cultures established only *TSC2*$^{+/+}$ colonies. These observations suggest that, within a bulk population those cells that express the highest levels of TSC2 will outcompete others in establishing pluripotent colonies, and further that cells completely devoid of TSC2 are incapable of epigenetic reprogramming to the pluripotent state. These findings are consistent with previous observations that hyperactive mTORC1 signaling is a barrier to iPSC reprogramming in mice, a phenomenon linked to a precise regulation of macroautophagy (41, 42), and establish TSC2 as an important mediator of reprogramming to pluripotency. It is particularly notable that *TSC2*$^{+/-}$ iPSC colonies exhibit an increased propensity toward genomic instability (3 of 7 P6 *TSC2*$^{+/-}$ iPSC lines exhibited abnormal karyotypes, compared with only 2 of 12 iPSC lines derived from P5 and 00969 *TSC2*$^{+/+}$ dermal cells; Supplementary Fig. S2A and S2B). In addition, P6 tumor–derived iPSCs were unable to establish GATA6^{+}

Published OnlineFirst August 22, 2017; DOI: 10.1158/0008-5472.CAN-17-0925

endoderm cells *in vitro* (although endoderm-like tissue was observed *in vivo*; Supplementary Fig. S3A and S3D). In our extensive experience with iPSC culture and reprogramming using cells derived from both unaffected individuals and those with various genetic diseases, we have never before observed karyotypic and developmental abnormalities to this magnitude (14, 43–46). Together, these data suggest that TSC2 is required for reprogramming to pluripotency and that, while a half-maximal level of TSC2 is sufficient to establish iPSC colonies it sensitizes cells to atypically high levels of reprogramming-related stress. Strikingly, unpublished observations in our lab with TSC2-knockout hESCs generated by genome editing have revealed that TSC2 is not similarly required to maintain pluripotency.

Consistent with other cellular models of LAM, P6-SMCs exhibit enhanced mTORC1 signaling, likely secondary to reduced TSC2 (11). However, compared with other models, which notably are fully TSC2-deficient ($TSC2^{-/-}$), but were not derived under SMC growth conditions (11), P6-N2 and tumor-derived SMCs express an increased number of mTOR- and LAM-associated features, including neural crest differentiation markers (e.g., GD3) and lymphangiogenesis biomarkers (VEGF-D; Table 1). In addition, tumor-derived lines are uniquely sensitive to combined mTORC1 and autophagy inhibition (Table 1). These differences strongly suggest that selection of *TSC2* mutation-bearing cells under SMC growth conditions promotes the isolation and expansion of cells with potent LAM-like phenotypes, whether they are $TSC2^{+/-}$ or $TSC2^{-/-}$. This highlights the importance of employing the appropriate supportive culture conditions to promote the selection and expansion of desired cell types (typically tumor and disease-related cells) from heterogenous populations. The LAM-associated phenotypes observed in P6-SMC cultures, including expression of the melanocyte marker GD3, support the hypothesis that LAM cells are associated with the neural crest-SMC lineage (28, 29, 47). Given that the TSC-LAM patient-derived teratomas exhibited multi-lineage differentiation, it is foreseeable that cell types associated with other TSC-associated lesions, specifically the neural and broader neural crest lineages (1), may be isolated by culturing patient iPSC-derived teratoma tissue under culture conditions supportive of these lineages.

Intriguingly, $TSC2^{+/-}$ P6-SMCs demonstrate haploinsufficiency, as they exhibit a majority of the molecular, morphologic, and metabolic features attributed to LAM cells, which are typically considered to be *TSC2*-null. Thus, it is possible that $TSC2^{+/-}$ cells may potentiate disease phenotypes within LAM nodules. Our observations align with recent studies showing that $TSC2^{+/-}$ cells can exhibit some disease-associated phenotypes and may contribute to pathology in TSC and LAM (20–23), and that *TSC2*-expressing cells can acquire aberrant phenotypes when associated with *TSC2*-deficient cells (48). It is important to note, however, that while some phenotypes were unchanged (e.g., gp100 and ERα expression; Supplementary Fig. S6), further reduction of *TSC2* in P6-SMCs led to a substantial elevation in LAM-associated mTORC1 activity (Supplementary Fig. S5); thus, the full extent of LAM-associated phenotypes might only be observed in

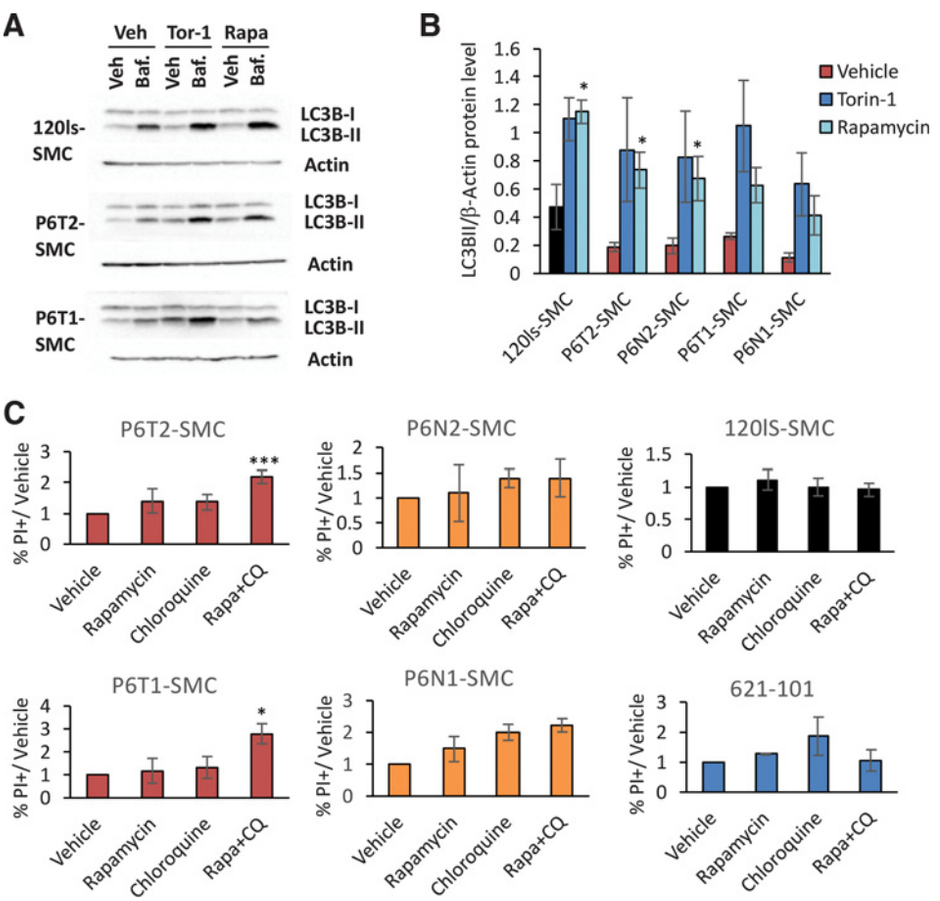

Figure 6.
Selective toxicity of TSC-LAM patient SMCs by dual targeting of mTORC1 and autophagy signaling. **A,** Representative Western blots of LC3B-I and LC3B-II levels in control (120ls-SMCs) and P6-derived SMC lines to depict LC3B-II accumulation in vehicle versus +bafilomycin A1 conditions, and the corresponding response to mTOR inhibitors torin-1 and rapamycin. **B,** Basal levels of LC3B-II, based on densitometry quantification of Western blots and normalized to β-actin levels, in SMC lines under vehicle, torin-1, or rapamycin treatment. Statistics are relative to vehicle. **C,** Percent of cells positive for propidium iodide (PI) relative to vehicle for each cell line, following a 24-hour treatment with 2.5 μmol/L chloroquine (CQ), 20 nmol/L rapamycin, or both. Measurements were collected via flow cytometry. *, $P < 0.05$ and ***, $P < 0.001$, obtained by *t* test, are indicated. Three biological replicates were performed for each experiment and treatment condition.

Published OnlineFirst August 22, 2017; DOI: 10.1158/0008-5472.CAN-17-0925

TSC2$^{-/-}$ cells. In agreement, while results were similar across all four P6-derived cell lines for most of the mTOR- and LAM-associated assays we conducted, some phenotypes were apparent in only a subset of the P6-SMC lines (e.g., elevated HIF1α and GD3 expression, specific metabolic features). In addition, while combined rapamycin and chloroquine treatment caused toxicity in tumor-derived SMC lines, these effects were relatively modest (Fig. 6C). Thus, while *TSC2*$^{+/-}$ SMCs show potential utility in drug screens aimed at identifying molecules that selectively kill LAM cells, *TSC2*$^{-/-}$ SMCs will likely be optimal, underscoring the need for the establishment of *TSC2*-knockout cell lines via approaches such as genome engineering.

Although P6-SMC lines appear to be genetically identical based on our sequencing analyses, the tumor-derived lines express some phenotypes not observed in the normal dermal-derived lines, most notably sensitivity to combined mTORC1 and autophagy inhibition. Thus, it seems likely that the P6 tumor–derived SMCs have retained some epigenetic memory, a phenomenon previously documented in reprogrammed iPSC lines (19), which is associated with their original identity as tumor cells. This suggests that tumor-derived cells, and likely also those that are *TSC2*-null, are most appropriate for establishing TSC- and LAM-like cell lines suitable for disease modeling and drug screening studies. In addition, only the P6T1-SMC line exhibited all LAM-like features that we evaluated, while other lines lacked 1–3 key features. This highlights a moderate level of clone-specific phenotypic variability and, consequently, the importance of screening multiple clones in patient-derived cell panels to identify the best candidates. However, as our four P6-SMC lines are still highly similar to one another, we believe our approach represents a robust and reproducible method of establishing disease-relevant cell lines.

In summary, we have used iPSC technology to shed light on the developmental and genetic events required for the evolution of LAM cells and tumors. In doing so, we have developed a novel and relevant patient-derived cell model of LAM, as well as a unique technical approach to selecting and expanding *TSC2* mutation–bearing LAM-like cells. TSC–mTORC1 signaling is a central component of the physiology of all cells and is involved in a multitude of developmental processes (1, 49). Accordingly, dysregulation of this pathway is implicated in a number of cancer syndromes and human diseases (49). Thus, our findings of essential roles of TSC2 in establishing pluripotency and in driving (LAM) disease–related phenotypes in a (SMC) lineage-dependent manner have broad implications for our understanding of both development and cell fate regulation, and offer important insights for the generation of additional human cell–based models of disease.

Disclosure of Potential Conflicts of Interest

No potential conflicts of interest were disclosed.

Authors' Contributions

Conception and design: L.M. Julian, S.P. Delaney, Y. Wang, A.A. Goldberg, E.P. Henske, A.S. Kristof, W.L. Stanford

Development of methodology: L.M. Julian, S.P. Delaney, Y. Wang, A.A. Goldberg, J. Yockell-Lelièvre, M.-E. Harper, E.P. Henske, A.S. Kristof, W.L. Stanford

Acquisition of data (provided animals, acquired and managed patients, provided facilities, etc.): S.P. Delaney, Y. Wang, A.A. Goldberg, J. Yockell-Lelièvre, R.Y. Tam, K. Giannikou, F. McMurray, M.-E. Harper, D.J. Kwiatkowski, J. Moss, A.S. Kristof

Analysis and interpretation of data (e.g., statistical analysis, biostatistics, computational analysis): L.M. Julian, S.P. Delaney, Y. Wang, A.A. Goldberg, C. Doré, J. Yockell-Lelièvre, K. Giannikou, F. McMurray, M.-E. Harper, D.J. Kwiatkowski, A.S. Kristof, W.L. Stanford

Writing, review, and/or revision of the manuscript: L.M. Julian, S.P. Delaney, Y. Wang, A.A. Goldberg, J. Yockell-Lelièvre, R.Y. Tam, K. Giannikou, M.S. Shoichet, M.-E. Harper, E.P. Henske, D.J. Kwiatkowski, T.N. Darling, J. Moss, A.S. Kristof, W.L. Stanford

Administrative, technical, or material support (i.e., reporting or organizing data, constructing databases): S.P. Delaney, Y. Wang, C. Doré, R.Y. Tam, T.N. Darling, A.S. Kristof

Study supervision: L.M. Julian, A.S. Kristof, W.L. Stanford

Other (initial derivation and characterization of cells from human samples): T.N. Darling

Acknowledgments

We wish to thank Kamal Garcha for his early work on this project and Catherine Lawrence for her inspiration. We would also like to thank the RI-MUHC Histopathology Platform for their help.

Grant Support

This research was supported by a Special Accelerated Discovery grant by the McEwen Centre for Regenerative Medicine, supported by Green Eggs and LAM (to W.L. Stanford and M.S. Shoichet), and a grant W81XWH-14-1-0434 (awarded to W.L. Stanford and A.S. Kristof) from the United States Department of Defense via the Tuberous Sclerosis Complex Research Program of the Congressionally Directed Medical Research Program. Salary support for Y. Wang, A. Goldberg, C. Doré, J. Yockell-Lelièvre, and R.Y. Tam was provided through these grants. Research reported in this publication was additionally supported by the National Institute of Arthritis and Musculoskeletal and Skin Diseases of the NIH (award #R01AR062080 to T.N. Darling), the Canadian Institutes of Health Research (FDN 143278 to M. Harper), and the Intramural Research Program, NIH, National Heart, Lung, and Blood Institute (to J. Moss). We are grateful for support from the LAM Foundation and LAM Canada (to A.S. Kristof), and from the Lucy J. Engles TSC/LAM Research Program (to E.P. Henske and D.J. Kwiatkowski). L.M. Julian was supported by Ontario Institute for Regenerative Medicine and CIHR Banting Postdoctoral Fellowships, S.P. Delaney by a Judith R. Raymond Scholarship in Cancer Research, A. Goldberg by a Richard and Edith Strauss Fellowship in Respiratory Medicine, and F. McMurray by a Destination 2020 University of Ottawa and Ontario Ministry of Research Fellowship. W.L. Stanford was funded by a Tier 1 Canada Research Chair in Integrative Stem Cell Biology.

The costs of publication of this article were defrayed in part by the payment of page charges. This article must therefore be hereby marked *advertisement* in accordance with 18 U.S.C. Section 1734 solely to indicate this fact.

Received April 5, 2017; revised June 22, 2017; accepted August 16, 2017; published OnlineFirst August 22, 2017.

References

1. Delaney SP, Julian LM, Stanford WL. The neural crest lineage as a driver of disease heterogeneity in tuberous sclerosis complex and lymphangioleiomyomatosis. Front Cell Dev Biol 2014;2:69.
2. Henske EP, Jozwiak S, Kingswood JC, Sampson JR, Thiele EA. Tuberous sclerosis complex. Nat Rev Dis Primers 2016;2:16035.
3. Grzegorek I, Lenze D, Chabowski M, Janczak D, Szolkowska M, Langfort R, et al. Immunohistochemical evaluation of pulmonary lymphangioleiomyomatosis. Anticancer Res 2015;35:3353–60.
4. Henske EP, McCormack FX. Lymphangioleiomyomatosis—a wolf in sheep's clothing. J Clin Invest 2012;122:3807–16.
5. Gao L, Yue MM, Davis J, Hyjek E, Schuger L. In pulmonary lymphangioleiomyomatosis expression of progesterone receptor is frequently higher than that of estrogen receptor. Virchows Archiv 2014;464:495–503.
6. Logginidou H, Ao X, Russo I, Henske EP. Frequent estrogen and progesterone receptor immunoreactivity in renal angiomyolipomas from women with pulmonary lymphangioleiomyomatosis. Chest 2000;117:25–30.

Published OnlineFirst August 22, 2017; DOI: 10.1158/0008-5472.CAN-17-0925

7. Ando K, Kurihara M, Kataoka H, Ueyama M, Togo S, Sato T, et al. Efficacy and safety of low-dose sirolimus for treatment of lymphangioleiomyomatosis. Respir Investig 2013;51:175–83.
8. Darling TN, Pacheco Rodriguez G, Gorio A, Lesma E, Walker C, Moss J. Lymphangioleiomyomatosis and TSC2−/− cells. Lymphat Res Biol 2010;8:59–69.
9. Kwiatkowski DJ. Animal models of lymphangioleiomyomatosis (LAM) and tuberous sclerosis complex (TSC). Lymphat Res Biol 2010;8:51–7.
10. Arbiser JL, Yeung R, Weiss SW, Arbiser ZK, Amin MB, Cohen C, et al. The generation and characterization of a cell line derived from a sporadic renal angiomyolipoma: use of telomerase to obtain stable populations of cells from benign neoplasms. Am J Pathol 2001;159:483–91.
11. Yu J, Astrinidis A, Howard S, Henske EP. Estradiol and tamoxifen stimulate LAM-associated angiomyolipoma cell growth and activate both genomic and nongenomic signaling pathways. Am J Physiol Lung Cell Mol Physiol 2004;286:L694–700.
12. Avior Y, Sagi I, Benvenisty N. Pluripotent stem cells in disease modelling and drug discovery. Nat Rev Mol Cell Biol 2016;17:170–82.
13. Tyburczy ME, Wang JA, Li S, Thangapazham R, Chekaluk Y, Moss J, et al. Sun exposure causes somatic second-hit mutations and angiofibroma development in tuberous sclerosis complex. Hum Mol Genet 2014;23:2023–9.
14. Chang WY, Lavoie JR, Kwon SY, Chen Z, Manias JL, Behbahani J, et al. Feeder-independent derivation of induced-pluripotent stem cells from peripheral blood endothelial progenitor cells. Stem Cell Res 2013;10: 195–202.
15. Chen Z, Chang WY, Etheridge A, Strickfaden H, Jin Z, Palidwor G, et al. Reprogramming progeria fibroblasts re-establishes a normal epigenetic landscape. Aging Cell 2017;16:870–87.
16. Uphoff CC, Drexler HG. Detection of mycoplasma contaminations. Methods Mol Biol 2005;290:13–23.
17. Okita K, Matsumura Y, Sato Y, Okada A, Morizane A, Okamoto S, et al. A more efficient method to generate integration-free human iPS cells. Nat Methods 2011;8:409–12.
18. Chen G, Gulbranson DR, Hou Z, Bolin JM, Ruotti V, Probasco MD, et al. Chemically defined conditions for human iPSC derivation and culture. Nat Methods 2011;8:424–9.
19. Kim K, Doi A, Wen B, Ng K, Zhao R, Cahan P, et al. Epigenetic memory in induced pluripotent stem cells. Nature 2010;467:285–90.
20. D'Armiento J, Shiomi T, Marks S, Geraghty P, Sankarasharma D, Chada K. Mesenchymal tumorigenesis driven by TSC2 haploinsufficiency requires HMGA2 and is independent of mTOR pathway activation. Cancer Res 2016;76:844–54.
21. Wilson C, Bonnet C, Guy C, Idziaszczyk S, Colley J, Humphreys V, et al. Tsc1 haploinsufficiency without mammalian target of rapamycin activation is sufficient for renal cyst formation in Tsc1+/− mice. Cancer Res 2006;66:7934–8.
22. Costa V, Aigner S, Vukcevic M, Sauter E, Behr K, Ebeling M, et al. mTORC1 inhibition corrects neurodevelopmental and synaptic alterations in a human stem cell model of tuberous sclerosis. Cell Rep 2016;15:86–95.
23. Peri S, Caretti E, Tricarico R, Devarajan K, Cheung M, Sementino E, et al. Haploinsufficiency in tumor predisposition syndromes: altered genomic transcription in morphologically normal cells heterozygous for VHL or TSC mutation. Oncotarget 2016;8:17628–42.
24. Xie CQ, Zhang J, Villacorta L, Cui T, Huang H, Chen YE. A highly efficient method to differentiate smooth muscle cells from human embryonic stem cells. Arterioscler Thromb Vasc Biol 2007;27:e311–2.
25. Shim B, Pacheco Rodriguez G, Kato J, Darling TN, Vaughan M, Moss J. Sex-specific lung diseases: effect of oestrogen on cultured cells and in animal models. Eur Respir Rev 2013;22:302–11.
26. Parkhitko A, Myachina F, Morrison TA, Hindi KM, Auricchio N, Karbowniczek M, et al. Tumorigenesis in tuberous sclerosis complex is autophagy and p62/sequestosome 1 (SQSTM1)-dependent. Proc Natl Acad Sci U S A 2011;108:12455–60.
27. Taveira-DaSilva AM, Moss J. Clinical features, epidemiology, and therapy of lymphangioleiomyomatosis. Clin Epidemiol 2015;7:249–57.
28. Zhe X, Schuger L. Combined smooth muscle and melanocytic differentiation in lymphangioleiomyomatosis. J Histochem Cytochem 2004; 52:1537–42.
29. Matsumoto Y, Horiba K, Usuki J, Chu SC, Ferrans VJ, Moss J. Markers of cell proliferation and expression of melanosomal antigen in lymphangioleiomyomatosis. Am J Respir Cell Mol Biol 1999;21:327–36.
30. Gilbert ER, Eby JM, Hammer AM, Klarquist J, Christensen DG, Barfuss AJ, et al. Positioning ganglioside D3 as an immunotherapeutic target in lymphangioleiomyomatosis. Am J Pathol 2013;183:226–34.
31. Hoon V, Thung SN, Kaneko M, Unger PD. HMB-45 reactivity in renal angiomyolipoma and lymphangioleiomyomatosis. Arch Pathol Lab Med 1994;118:732–4.
32. Finlay G. The LAM cell: what is it, where does it come from, and why does it grow? Am J Physiol Lung Cell Mol Physiol 2004;286:L690–3.
33. Juvet SC, McCormack FX, Kwiatkowski DJ, Downey GP. Molecular pathogenesis of lymphangioleiomyomatosis: lessons learned from orphans. Am J Respir Cell Mol Biol 2007;36:398–408.
34. Young L, Lee HS, Inoue Y, Moss J, Singer LG, Strange C, et al. Serum VEGF-D a concentration as a biomarker of lymphangioleiomyomatosis severity and treatment response: a prospective analysis of the Multicenter International Lymphangioleiomyomatosis Efficacy of Sirolimus (MILES) trial. Lancet Respir Med 2013;1:445–52.
35. Young LR, Vandyke R, Gulleman PM, Inoue Y, Brown KK, Schmidt LS, et al. Serum vascular endothelial growth factor-D prospectively distinguishes lymphangioleiomyomatosis from other diseases. Chest 2010;138:674–81.
36. Cao J, Tyburczy ME, Moss J, Darling TN, Widlund HR, Kwiatkowski DJ. Tuberous sclerosis complex inactivation disrupts melanogenesis via mTORC1 activation. J Clin Invest 2017;127:349–64.
37. Choo AY, Kim SG, Vander Heiden MG, Mahoney SJ, Vu H, Yoon SO, et al. Glucose addiction of TSC null cells is caused by failed mTORC1-dependent balancing of metabolic demand with supply. Mol Cell 2010;38:487–99.
38. Inoki K, Zhu T, Guan K-L. TSC2 mediates cellular energy response to control cell growth and survival. Cell 2003;115:577–90.
39. Sun Y, Gu X, Zhang E, Park MA, Pereira AM, Wang S, et al. Estradiol promotes pentose phosphate pathway addiction and cell survival via reactivation of Akt in mTORC1 hyperactive cells. Cell Death Dis 2014;5: e1231.
40. Parkhitko AA, Priolo C, Coloff JL, Yun J, Wu JJ, Mizumura K, et al. Autophagy-dependent metabolic reprogramming sensitizes TSC2-deficient cells to the antimetabolite 6-aminonicotinamide. Mol Cancer Res 2014;12:48–57.
41. Wu Y, Li Y, Zhang H, Huang Y, Zhao P, Tang Y, et al. Autophagy and mTORC1 regulate the stochastic phase of somatic cell reprogramming. Nat Cell Biol 2015;17:715–25.
42. Wang S, Xia P, Ye B, Huang G, Liu J, Fan Z. Transient activation of autophagy via Sox2-mediated suppression of mTOR is an important early step in reprogramming to pluripotency. Cell Stem Cell 2013;13:617–25.
43. McDonald AC, Biechele S, Rossant J, Stanford WL. Sox17-mediated XEN cell conversion identifies dynamic networks controlling cell-fate decisions in embryo-derived stem cells. Cell Rep 2014;9:780–93.
44. Kinnear C, Chang WY, Khattak S, Hinek A, Thompson T, de Carvalho Rodrigues D, et al. Modeling and rescue of the vascular phenotype of Williams-Beuren syndrome in patient induced pluripotent stem cells. Stem Cells Transl Med 2013;2:2–15.
45. Shelton M, Kocharyan A, Liu J, Skerjanc IS, Stanford WL. Robust generation and expansion of skeletal muscle progenitors and myocytes from human pluripotent stem cells. Methods 2016;101:73–84.
46. Hotta A, Cheung AY, Farra N, Garcha K, Chang WY, Pasceri P, et al. EOS lentiviral vector selection system for human induced pluripotent stem cells. Nat Protoc 2009;4:1828–44.
47. Corrin B, Liebow AA, Friedman PJ. Pulmonary lymphangiomyomatosis. A review. Am J Pathol 1975;79:348–82.
48. Patel B, Patel J, Cho JH, Manne S, Bonala S, Henske E, et al. Exosomes mediate the acquisition of the disease phenotypes by cells with normal genome in tuberous sclerosis complex. Oncogene 2016;35:3027–36.
49. Laplante M, Sabatini DM. mTOR signaling in growth control and disease. Cell 2012;149:274–93.

Cancer Research
The Journal of Cancer Research (1916–1930) | The American Journal of Cancer (1931–1940)

AACR American Association for Cancer Research

Human Pluripotent Stem Cell–Derived *TSC2*-Haploinsufficient Smooth Muscle Cells Recapitulate Features of Lymphangioleiomyomatosis

Lisa M. Julian, Sean P. Delaney, Ying Wang, et al.

Cancer Res 2017;77:5491-5502. Published OnlineFirst August 22, 2017.